EPJ Web of Conferences **155**, 00006 (2017) DOI: 10.1051/epjconf/201715500006
JDN 22

Diffuse scattering

Isabelle Mirebeau[a]

Laboratoire Léon Brillouin, CEA-CNRS, CE-Saclay, 91191 Gif-sur-Yvette, France

Abstract. Diffuse neutron scattering covers a wide range of phenomena related to short range nuclear and magnetic orderings. Although it is "a priori" simple to measure, the underlying physics is often quite complex. Extracting useful and reliable information requires careful corrections and calibrations, and appropriate models of analysis, specifics for each physical case. This paper yields a partial and subjective glance on this specific subject, showing studies about chemical orderings in binary alloys and magnetic correlations in frustrated "spin ices" as examples.

1. Introduction

In reciprocal space, the term "diffuse scattering" covers scattering processes which extend on a large part of the Brillouin zone. It therefore contrasts with "Bragg scattering" which is limited to the vectors of the reciprocal space, and with "small angle scattering" which covers a small portion of the reciprocal space surrounding the zone center (typically up to 0.1 $Å^{-1}$). Neutron scientists have usually reserved the term of "diffuse scattering" to a diffraction process, measured in the so called "two axis" geometry, without performing an energy analysis of the scattered neutron beam. For fluctuating phenomena, this means that one basically measures the instantaneous correlations, taking a "snapshot" of the system. In many cases however, the process of interest is of elastic nature, as it involves static configurations. Recent measurements also select the elastic contribution by performing an energy analysis of the scattered beam using time of flight techniques for instance.

In real space, diffuse scattering allows one to investigate a large variety of states of imperfect matter, where defects range at a local scale, in opposition to the long range periodic order and to the mesoscopic order studied through Bragg and small angle scattering processes respectively. Actually any real sample is imperfect when one studies it sufficiently closely, and the experiment looks quite simple: one just measures everything between the Bragg peaks! Therefore, for a long time, diffuse scattering measurements have been considered in a rather despising way as "scraping the background". The difficulty arises when one wants to extract reliable information from this diffuse "background", coming from the phenomenon of interest. This requires extracting the relevant signal from all other sources of environmental and physical background contributions. This procedure may require the calibration of the measured signal in absolute scale, and a comparison with an "*a priori*" model to refine the relevant parameters. Such refinements may be complex, since there is no general procedure such as those developed to analyze long range periodic order, so that each physical case is specific and yields its own method of analysis.

Which states of matter can be studied through diffuse scattering? Actually there are no limitations in the states of disorder or local order which can be investigated in solid

[a] e-mail: isabelle.mirebeau@cea.fr

state physics. The great advantage of the neutron probe is the possibility to investigate the bulk state, and to study nuclear and magnetic correlations separately. As for nuclear scattering, one can quote studies of local occupation disorder in solid solutions and alloys, initiated by the pioneering work of Cowley and Warren [1], static local displacements initially modelled by Borie and Sparks [2], orientation disorder, local defects in quasi-crystals or aperiodic materials [3] among others. In all these studies, an underlying periodic or quasi-periodic lattice is postulated. Amorphous and liquid states also yield diffuse scattering, but specific tools of analysis have been developed in such cases which will not be mentioned here. As for the magnetic scattering, one can quote studies of magnetic correlations above a critical transition, the determination of local moments and local perturbations in ferromagnetic alloys [4], investigations of 2D and 1D systems [5], Bose condensates with dimer ordering [6], magnetic fluctuations in unconventional superconductors [7], and the large variety of entropic disordered ground states observed in frustrated systems, such as spin liquids, spin ices, or spin glasses [8], among others.

In the following, this chapter starts to provide a few guidelines about the necessary corrections, which could be helpful for who discovers the technique, and briefly mentions the general descriptions developed as a first approach, depending on the reference state (fully ordered or fully random). An example of the progressive evolution from order to disorder is shown by the quantum critical transition from canted ferrimagnetism to spin-glass states in molybdate pyrochlores. Then one focuses on a few examples where neutron diffuse scattering was modeled and yielded useful information. These examples deal with binary alloys with site disorder, and with the exotic local magnetic order shown by the "spin ices".

2. How to measure diffuse scattering? Experimental corrections

Measurements of the diffuse scattering are usually done on a two axis spectrometer. For powder, one uses a powder diffractometer equipped with a multidetector, whereas for single crystals several geometries can be used. The most common one involves multi-counters in the scattering plane such as D7 at the ILL [9], allowing one to scan a given fraction of the desired scattering plane by rotating an oriented crystal along a vertical axis (the so-called "snail curves"). In some cases, polarized neutrons are used to separate nuclear from magnetic scattering contributions. In ferromagnetic alloys, unpolarized neutron measurements combining different orientations of the saturating magnetic field are an interesting alternative.

The procedure to determine the diffuse scattering contributions arising from magnetic and nuclear short range order in a ferromagnetic alloy is given here as an example of the typical corrections which should be performed. The sample is measured at low temperature, typically 2 to 5 K, to eliminate the contribution of phonons, and for two geometries of the magnetic field **H**: in zero field corresponding to random orientations of the ferromagnetic domains; under a saturating field $\mathbf{H}_{sat}$ perpendicular to the scattering plane, to obtain a single domain oriented perpendicular to all **Q** vectors.

The intensities of the empty sample holder (E), vanadium sample (V), and fully absorbing cadmium sample (Cd) are also measured with the same experimental set-up. To minimize the corrections, Vanadium and Cadmium samples occupy the same volume as the studied sample (assumed here to be a cylinder with radius R and length L, with $L \gg R$). The following formula accounts for: 1) the correction from the environmental background due to the neutron beam after traversing the sample (E-Cd) and from the background outside the sample (Cd); 2) the detector efficiency; 3) the absorption correction [10]; 4) the multiple scattering corrections [11]; 5) an absolute calibration, taking the incoherent scattering of vanadium as a reference.

Absorption and multiple scattering corrections are tabulated for a cylindrical sample and for standard geometries, knowing the absorption coefficient $\mu = n\sigma_T$ (where n_S is the sample density and σ_T the *total* sample cross section estimated for the incident neutron wavelength of the experiment, from the cross sections of the individual constituents) [12]. In the case of complicated shapes, a Monte-Carlo correction has to be used to account for the absorption and multiple scattering of all trajectories inside the sample, given the incident and exit directions. Corrections taking inelastic scattering into account through Monte Carlo codes have been also developed [11].

The corrected intensity scattered by the sample N_S^{cor} is given by:

$$N_S^{cor} = N_S - N_{Cd} - A_S(0)[N_E - N_{Cd}]$$

where N_S, N_E and N_{Cd} are the intensities recorded from the sample, the empty sample holder and a Cd sample of the same volume respectively, for the same number of incident neutrons. A(0) is the transmission coefficient.

The neutron scattering cross section is given in absolute units by:

$$\frac{d\sigma}{d\Omega}(\mathbf{Q}) = \frac{\sigma_{inc}}{4\pi}\frac{n_V}{n_S}\frac{A_V(\theta)}{A_S(\theta)}\frac{(1-\delta_S^{'})}{(1-\delta_V^{'})}\frac{N_S^{cor}(\theta)}{N_V^{cor}(\theta)}$$

where $\sigma_{inc} = 5.07$ barn is the incoherent cross section of vanadium; n_S and n_V are the sample and vanadium number of atoms, as deduced from the mass of the measured samples; $A(\theta)$ is the absorption coefficient and 2θ the scattering angle; δ_S' and δ_V' are the multiple scattering coefficients of the sample and vanadium.

From the total cross section, the magnetic and nuclear diffuse cross sections are given by:

$$\frac{d\sigma}{d\Omega}(\mathbf{Q}) = \frac{d\sigma_N}{d\Omega}(\mathbf{Q}) + \frac{2}{3}\frac{d\sigma_M}{d\Omega}(\mathbf{Q}) \quad for\ \mathrm{H} = 0$$

$$\frac{d\sigma}{d\Omega}(\mathbf{Q}) = \frac{d\sigma_N}{d\Omega}(\mathbf{Q}) + \frac{d\sigma_M}{d\Omega}(\mathbf{Q}) \quad for\ \mathbf{H} \perp \mathbf{Q}$$

some other configurations can be used: i) measurements in a field along the scattering vector $\mathbf{Q}$ ($\mathbf{H}$ // $\mathbf{Q}$); ii) polarized neutron measurements, with $\mathbf{P}_Z$ either parallel or antiparallel to the saturating field ($\mathbf{H} \perp \mathbf{Q}$). They yield the following equations:

$$\frac{d\sigma}{d\Omega}(\mathbf{Q}) = \frac{d\sigma_N}{d\Omega}(\mathbf{Q}) \quad for\ \mathbf{H}//\mathbf{Q}$$

$$\frac{d\sigma}{d\Omega}(\mathbf{Q}) = \frac{d\sigma_N}{d\Omega}(\mathbf{Q}) + \frac{d\sigma_M}{d\Omega}(\mathbf{Q}) \pm \frac{d\sigma_{NM}}{d\Omega}(\mathbf{Q}).$$

These equations may be combined to extract the differential cross sections $\frac{d\sigma_N}{d\Omega}(\mathbf{Q})$, $\frac{d\sigma_M}{d\Omega}(\mathbf{Q})$, $\frac{d\sigma_{NM}}{d\Omega}(\mathbf{Q})$ corresponding to the nuclear, magnetic and interference terms respectively.

Using this procedure, one can calibrate the diffuse intensity without using the Bragg scattering as a reference. This is important since there might be no Bragg scattering from the sample if one uses a large incident wavelength to measure the diffuse scattering with a good resolution. Moreover, diffuse scattering measurements are usually performed on large single crystals in "two-axis" geometry, so the Bragg intensities can be strongly affected by extinction effects or by imperfect sample orientation. This method was used to study the local chemical and magnetic orders in solid solutions of Fe, Ni or Co based ferromagnetic alloys, among others.

In the case of dilute Fe-Cr alloys (see paragraph 4 below), where the nuclear signal from local Cr order is very small due to the small contrast between Cr and Fe atoms, the same $Fe_{0.95}Cr_{0.05}$ sample was measured twice, with different background conditions [13].

In the first set-up the intensity coming from the sample was well below that of the environmental background (mostly the air scattered by the incident neutron beam) and the sample signal could not be detected without performing all corrections. By using a vacuum chamber compatible with a cryostat and an electromagnet, the second set-up decreased the environmental background by about a factor 20, allowing a direct visualization of the sample signal, a better precision of the neutron cross section yielding the determination of short range order parameters over further neighbor distances, and measurements at lower Cr contents. Although the statistical precision was significantly improved in the second case, suitable corrections and calibrations yielded the same value of the average cross section in absolute scale for both set-ups, which compares well with the calculated sum of the incoherent and Laue scattering cross sections. This allowed the nearest neighbor short range order parameters to be determined in any case.

3. How to describe diffuse scattering? A few guidelines

Usually the diffuse scattering signal is described either as a deviation from the Long Range Ordered state (LRO yielding Bragg scattering) or as a deviation from the fully disordered or random state (yielding incoherent Laue scattering or uncorrelated paramagnetic scattering). In other words, the Q dependence of the diffuse intensity I(Q) is simulated either by a broadening of the Bragg peaks, or by modulations of the flat incoherent "background" between them. The first method which takes LRO as a reference yields the determination of correlations lengths, typical domain size, critical behaviors [14], long ranged distortions [15], in some cases quantum fluctuations or spin waves constants [5, 16]. It is well adapted to typical length scales of a few tens of unit cells. The second method, taking the random state as a reference, yields the determination of short range order nuclear parameters [1, 13, 17–20], short range ordering of vacancies [21], local magnetic perturbations [22], local lattice distortions [2, 21], or pair distribution functions [23]. It covers atomic or spin correlations mostly limited to near neighbor distances. Examples of such cases are shown in paragraph 4 for $Fe_{1-x}Cr_x$ polycrystalline alloys and a FePd single crystal.

The choice of the appropriate description and reference state obviously depends on the context. As an example, Fig. 1 shows the evolution of the magnetic scattering from LRO to spin glass states across a quantum critical transition. This quantum transition which occurs in molybdate pyrochlores $(Tb_{1-x}La_x)_2Mo_2O_7$ can be encompassed either by *La* substitution which expands the lattice (Fig. 1 left) or by applied pressure which compresses the lattice (Fig. 1 right) [24]. Expanding the lattice yields a transition from spin glass to LRO, and the reverse occurs by lattice compression, due to the combined effects of a Mott transition and geometrical frustration [25]. At ambient pressure, in the spin glass sample ($x = 0$), the large sinusoidal modulations can be fitted by local magnetic parameters [26], yielding correlations over a few interatomic distances. Such correlations are either ferromagnetic (F) or antiferromagnetic (AF) depending on the magnetic pair concerned. At intermediate concentrations ($x = 0.1$), an intermediate mesoscopic order shown by Lorentzian line shapes develops over several unit cells at the positions of the Bragg peaks of the LRO, present in the $x = 0.2$ sample. This canted ferromagnetic LRO can be determined by refining the pattern of the $x = 0.2$ sample with the Fullprof suite [27], yielding the moment values and orientations in the ordered magnetic unit cell. The evolution of the peak line shapes shows that the two processes, chemical pressure versus applied pressure, are not fully equivalent. When applying pressure, the LRO is destroyed in an inhomogeneous way, likely due to pressure inhomogeneity, whereas a homogenous transition occurs under *La* substitution. The pattern of the $x = 0.2$ sample at 1.9 GPa shows the coexistence of Bragg peaks and sinusoidal modulations, respectively associated with LRO and near neighbor correlations. In contrast

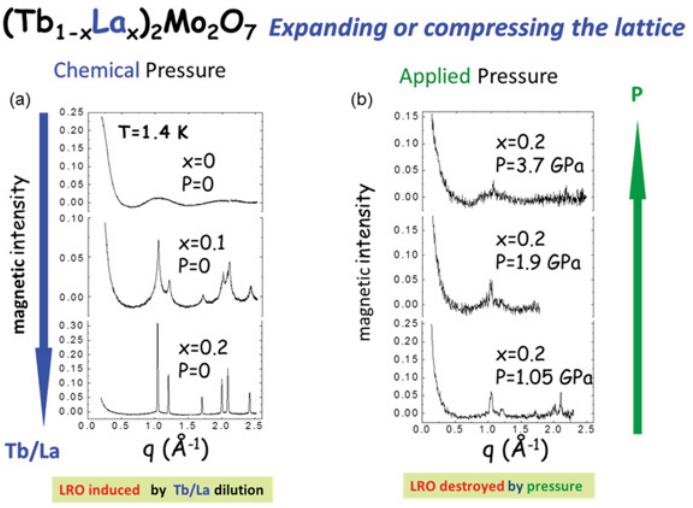

Figure 1. Evolution of the diffuse scattering through a quantum transition from spin glass to long range order in $(Tb_{1-x}La_x)_2Mo_2O_7$ pyrochlore alloys. The quantum transition can be encompassed either a) by chemical pressure (*La* substitution) or b) applied pressure. Note that the processes are different in the two cases, as shown by the intermediate magnetic phases at the middle part of the figures. Under chemical pressure ($x = 0.1, P = 0$), a mesoscopic phase appears with finite correlation length, as shown by the Lorentzian shape of the magnetic peaks. Under applied pressure ($x = 0.2, P = 1.9$ GPa), the intermediate state consists of short-range correlated regions (at the scale of a few interatomic distances) coexisting with a long-range magnetic ordering that involves a small ordered moment; from Ref. [24].

Lorentzian line shapes are observed in the $x = 0.1$ sample at ambient pressure, which can be related to the onset of homogeneous ordering over an intermediate length scale.

More recently new techniques have been developed to describe the diffuse scattering. For nuclear diffuse scattering, the determination of the pair distribution function (pdf) inspired by the studies of amorphous and liquid alloys, yields atomic pair correlations, interatomic distances, Debye-Waller coefficients and occupation numbers [26, 28]. It starts to be extended to the case of magnetic alloys [29]. Other methods based on Reverse Monte Carlo techniques [30] also allow one to obtain local magnetic correlations, assuming an energetic model and adjusting its parameters to obtain the best agreement with experiment. This is also the case of the inverse cluster variation method [31].

In some geometrically frustrated systems, such as spin ices, spin liquids or quantum spin ices, an original description of the short range ordered ground state and associated diffuse scattering has been very successful [8, 32, 33]. It is based on the postulate of conservation laws (such as the ice laws), yielding emergent electrodynamics and gauge fields. Postulating such laws is crucial, as it yields a description of a magnetic state different both from the paramagnetic state and from a long range ordered ground state. By giving a local conservation rule, one can define a fictitious field, obeying the general laws of electrodynamics. For classical Ising spins obeying "ice rules", this conservation law appear as a Gauss's law, and the associated electric field is directly linked with the classical spin. The dipolar character of the electric field in real space results in singularities of the magnetic structure factor in Fourier space. These highly anisotropic features show up as "bow-tie" features and "pinch-points", which can be directly observed in the Q-dependence of the neutron diffuse scattering. Flipping an individual spin violates the ice rules. These thermally activated excitations induce "magnetic monopoles", either source or sink of magnetic flux, which appear as a broadening

of the pinch points in the diffuse maps. For quantum spins, transverse energy terms (with respect to the Ising character), result in an effective field which has both electric and magnetic degree of freedom. The predicted excitations behave as particles of light. Observing these "emergent photons" in quantum spin ices constitutes a challenge of modern condensed matter physics. A brief insight on this fascinating subject, with some examples of the neutron diffuse scattering maps is given in paragraph 5.

4. Local chemical ordering in binary solid solutions

4.1 $Fe_{1-x}Cr_x$ alloys

$Fe_{1-x}Cr_x$ alloys are a unique case in nature showing an inversion of the short range atomic order within a solid solution. Namely the Cr atoms in a Fe matrix repel each other at low concentration, whereas they attract each other at high concentration. This feature seems to be at the origin of the peculiar mechanical properties shown by $Fe_{1-x}Cr_x$ alloys in the solid solution, which have important mechanical applications. There is presently a considerable effort in the search for materials highly resistant to radiation damages, which will be used both in future hybrid-type reactors and in future controlled fusion reactors. $Fe_{1-x}Cr_x$ alloys with base centered cubic (bcc) structure are the reference model to understand the behavior of ferritic FeCr based steels, considered as leading candidates in most future nuclear energy options. As a striking fact, the response of $Fe_{1-x}Cr_x$ alloys over irradiation is highly non monotonic, with a pronounced change of behavior around the critical concentration $x_c \sim 0.10$, where the short range order inversion takes place.

Understanding this behavior requires a precise knowledge of the pair interactions between the atoms which govern the distribution of the atoms over the lattice sites. In a solid solution, the atomic distribution is never fully random, and peculiar local configurations are privileged in a statistical way, controlled by the electronic configuration. In transition metal alloys, it has been known for decades that the electronic configuration energy can be written in terms of pair interactions [34].

Neutron diffuse scattering is the best way to determine the short range magnetic order in a solid solution. This is especially true for transition metal alloys of the first series, where the electronic contrast (difference of electronic numbers) that governs the amplitude of the X ray diffuse scattering intensity is quite small. Following a theoretical prediction based on the electronic band structure, neutron measurements were the first probe to observe the surprising inversion in $Fe_{1-x}Cr_x$. They were later confirmed by numerous experimental studies based on resistivity measurements, Mössbauer effect, thermoelectric power, enthalpy of formation, bulk modulus, irradiation by heavy ions, etc.. The initial band structure calculations were also followed by improved *ab initio* theories as well as extended Monte-Carlo simulations, confirming the validity of the pair potential approach.

How are short range order effects and short range order inversion shown up by neutron diffuse scattering? The visualisation of short range order is quite simple, since the nuclear cross section is the Fourier transform of the short range order Cawley-Warren parameters, which describe the statistical deviation of a local configuration with respect to that of a random distribution [1].

In a binary alloy $A_{1-x}B_x$, taking an A type atom at the origin, the atomic SRO parameter α_i is related to the conditional probability p_{AB} of having a B atom at a distance R_i:

$$\alpha_i = 1 - \frac{p_{AB}}{x} = 1 - \frac{p_{BA}}{1-x}.$$

A positive α_i value describes a tendency towards segregation ($p_{AB} < x$) over the i^{th} neighbour shell surrounding the A atom, whereas a negative value corresponds to a short range order

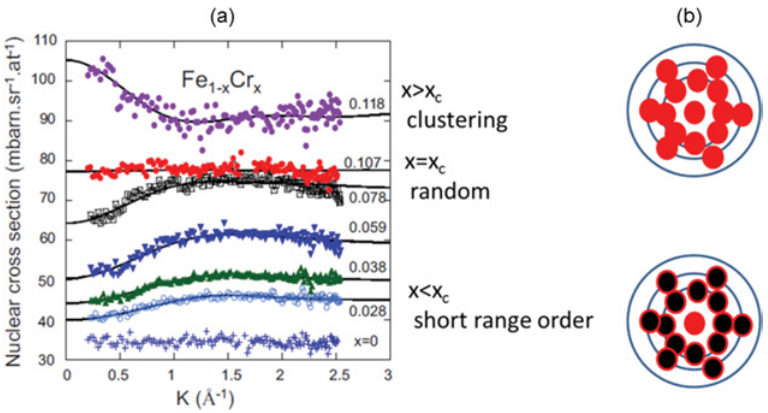

Figure 2. a) Neutron diffuse scattering in $Fe_{1-x}Cr_x$ alloys for different Cr contents x. A transition occurs at the critical concentration $x_c = 0.10$ At low concentration ($x<x_c$) the alloys tends to short range ordering (the neutron cross section decreases at low Q values). For $x=x_c$, the atomic distribution is random (the neutron cross section is flat). For $x>x_c$, the system tends to segregate (the neutron cross section increases at low Q values); b) schematic representation of the atomic distribution around a Cr atom (in red). From Ref. [13].

of hetero-coordination type ($p_{AB} > x$). In a single crystal, the neutron cross section is expressed by:

$$\frac{d\sigma}{d\Omega} = x(1-x)(b_A - b_B)^2 \sum \alpha(\boldsymbol{R_n}).\cos(\boldsymbol{Q}.\boldsymbol{R_n}).$$

Where b_A and b_B are the coherent scattering lengths associated with A and B species, and the sum extend over all pairs separated by a vector $\mathbf{R_n}$. One notices that in a single crystal, the intensity is periodic in reciprocal space. A tendency to segregation yields diffuse maxima located around $Q = 0$ and around the structural Bragg positions. A tendency towards "short range order" yields diffuse maxima located away from the structural peaks, usually around the peaks of an ordered superstructure. In a powder sample, the orientation average of the cosine term induces a loss of periodicity in the cross section, which is expressed by:

$$\frac{d\sigma}{d\Omega} = x(1-x)(b_A - b_B)^2 \left[1 + \sum_{i\neq 0}^{n} N_i \alpha_i \frac{\sin Q.R_i}{Q.R_i} \right].$$

Since the amplitude of the SRO parameters decreases with increasing R_i, the behaviour of the nuclear cross section at small Q-values is dominated by the sign of the first parameters. Depending on their sign, the modulations of the cross section suggest either a tendency towards a superstructure (onset of new Bragg peaks) or towards segregation (small angle scattering). Figure 2 shows the nuclear cross sections for a series of $Fe_{1-x}Cr_x$ alloys. At low concentrations, the nuclear cross section decreases at low Q values, whereas it increases at high concentrations. At the critical concentration $x_c = 0.01$, the cross section is Q-independent. This random distribution locates the short range order inversion.

Figure 3 (left) shows the variation of the first atomic SRO parameter α_{12} averaged over the first two neighbour shells. This average was necessary since the first two shells are close to each other in a bcc structure. At low Cr content, α_{12} is close to the limit value $-x/(1-x)$ which corresponds two maximum repulsion between Cr- Cr pairs, and it changes sign at the critical concentration. The experimental variation is compared with calculations from Monte Carlo simulations [35, 36]. In binary alloys, the configuration energy can be written in terms

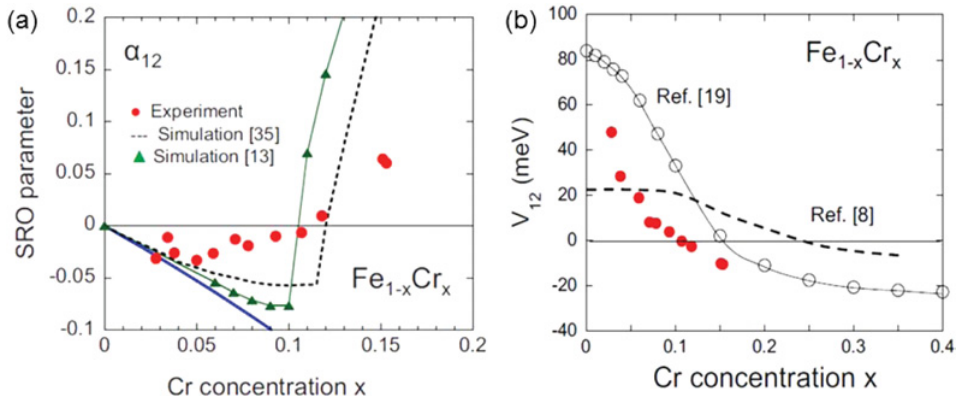

Figure 3. $Fe_{1-x}Cr_x$ alloys: a) variation of the first atomic short range order parameter, averaged over the first two neighbour distances of the base centred cubic lattice with Cr concentration x, from Ref. [13]. The experimental data are compared with the Monte-Carlo simulations of ref. [35, 36]; The solid blue line is the curve $-x/(1-x)$ of maximal repulsion between Cr-Cr pairs; b) variation of the first atomic pair potential V_{12} with Cr content, in comparison with ab initio calculations [38, 39].

of pair potentials and occupation parameters, via an Ising-like Hamiltonian. The minimisation of the free energy in mean field approximation [37] allows one to determine the effective pair potentials which govern the atomic interactions. In $Fe_{1-x}Cr_x$ alloys, the first pair potential V_{12} deduced from the SRO parameters also changes sign at x_c. In Fig. 3 (right), the experimental pair potential is compared with *ab initio* band structure calculations: the predictive behaviour of Ref. [38], and a more recent model [39].

4.2 FePd single crystal

In neutron diffuse scattering studies, the availability of a single crystal opens a route to a much more precise determination of the local order parameters and more detailed comparison with theory. Several extensive studies have been performed in the past, such as the investigation of ternary FeNiCr alloys [17], local order in CoPt [18] or FeV alloys [19], ordered vacancies in NiC [21] among others. A particular interesting case is the investigation of the diffuse scattering for a stoechiometric compound above the transition towards a LRO state. In such case, the analysis of the diffuse scattering allows one to predict the phase diagram, the ordering temperature and the nature of the LRO ground state. This is shown here in the case of cubic FePd [20]. Below the order-disorder temperature ($T_O = 920$ K), FePd alloys around the 50/50 stoechiometry order in the $L1_0$ structure, made of alternating pure Fe and pure Pd (001) planes. This strong anisotropy is accompanied with a magnetic anisotropy and tetragonal distortion. This phase transformation makes FePd alloys interesting as shape memory materials with potential applications as coupling devices.

Diffuse neutron scattering measurements were carried out in two reciprocal planes (100) and (110) at 1020 K, namely above T_O and in the paramagnetic state (well above the Curie temperature T_C =760 K), using time of flight energy analysis to extract the elastic signal from the dominant phonon contribution. The diffuse intensity, shown Fig. 4 is globally periodic in reciprocal space, and mainly located at the 100 and equivalent points, which correspond to the superstructure peaks of the $L1_0$ structure. A small asymmetry of the diffuse spots is due to local static displacements. The contribution from local *magnetic* order can be neglected, besides the ferromagnetic correlations between fluctuating Fe moments around the zone center, which have been discarded from the analysis. The SRO parameters (Fig. 4

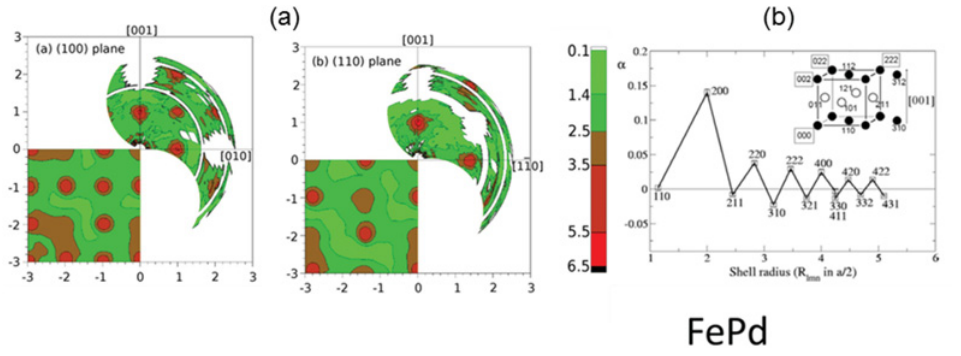

Figure 4. FePd single crystal: a) corrected diffuse experimental intensities in the (100) plane and (110) planes, and reconstructed intensities (down left for each figure) using SRO and lattice displacement parameters; b) variation of the SRO Cawley-Warren parameters versus the neighbour distances. The LRO structure of $L1_0$ type, with alternating pure Fe and pure Pd (001) planes, is shown in inset. From Ref. [20].

right) and lattice displacement parameters deduced from least square fit of the calibrated intensities extend to about 14 and 6 shells respectively. The calculation of the pair potentials from the SRO parameters was carried out using the cluster variation method (CVM) [31] which includes a description of the energy for a large set of clusters, going beyond the Bragg-Williams approximation used in the mean field model of Clapp and Moss [37]. The stability of the $L1_0$ phase is mainly due to the dominant second neighbour pair interactions, and the oscillating behaviour of the interactions between further neighbours.

5. Local magnetic ordering and coulomb phases in spin ices and quantum spin ices

Diffuse scattering has been one of the main tools to study spin ice behaviour in rare earth pyrochlores, starting from the pioneering experiments of Harris and Bramwell in $Ho_2Ti_2O_7$ [40]. In a spin ice, the magnetic moments are constrained by local Ising anisotropy to remain along the local 111 axes of the pyrochlore lattice, made of corner sharing tetrahedra. The minimization of the ferromagnetic exchange interaction within a given tetrahedron leads to the so-called "two in-two out" configuration (namely two spin pointing towards the center of the tetrahedron and two spin pointing outwards). This configuration can be mapped to the configuration which governs the hydrogen positions of water molecules in cubic ice, involving "two short and two long" hydrogen bond lengths in a given tetrahedron. Such configuration has six equivalent realizations. In the pyrochlore lattice of weakly connected tetrahedra, it yields a macroscopic extensive degeneracy of the ground state. As shown by Ramirez and co-workers [41], both water ice and spin ice ground states have the same configuration entropy at $T = 0$, governed by the ice rules. Another interesting mapping of the spin ice behaviour can be made with the "two up-two down" configuration which minimizes the energy of a Heisenberg antiferromagnet on the pyrochlore lattice [42].

In spin ices and similar materials, the magnetic moments become correlated at temperatures corresponding to the energy scale of the exchange interactions (given by the Curie-Weiss constant θ_{CW}), but a transition towards LRO does not occur. The magnetic ground state shows a very peculiar local ordering, due to the existence of strong constraints on the free energy [43]. Local rules govern the spin configurations and states with zero magnetization must maximize the entropy. These constraints result in an emergent gauge

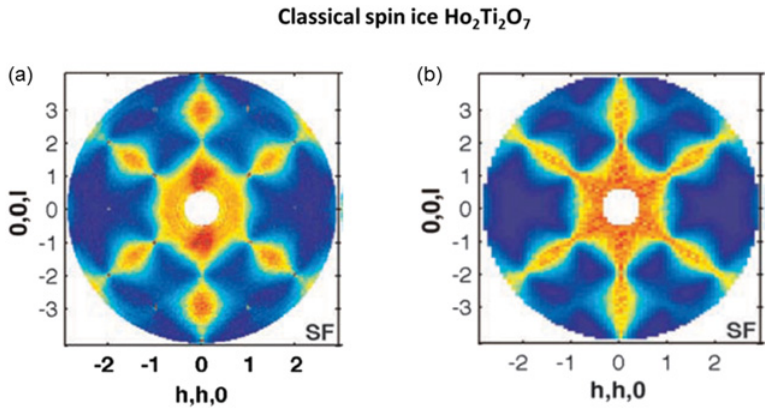

Figure 5. $Ho_2Ti_2O_7$ classical spin ice: a) experimental diffuse scattering map in a (110) plane measured by polarized neutrons in the spin flip channel; b): calculation in the dipolar spin ice model. From Ref. [44].

structure, (as in electrodynamics) and in a non-divergent magnetic field associated with the local rules governing the spin arrangements. As a consequence, the spatial variation of the spin correlations has an algebraic dependence similar to that of the dipolar interaction. In Fourier space, it corresponds to a very anisotropic shape of the diffuse scattering showing "pinch-points" or sharp bow-tie features [44].

The classical spin ice materials $Ho_2Ti_2O_7$ and $Dy_2Ti_2O_7$ which exist as large single crystals and possess large magnetic rare earth moments have enabled beautiful experiments probing this description. They are actually "dipolar spin ices", where the effective ferromagnetic first neighbour exchange is the sum of AF super-exchange and dipole-dipole interaction, the latter being screened for further neighbour distances. The strong Ising anisotropy coming from the crystal field scheme with ground state doublet well separated from the excited states constrains the spins along their local <111> axes. In this frame, the initial calculation of the neutron diffuse scattering maps by Monte Carlo simulation and comparison with the experimental maps was the first proof of the validity of dipolar spin ice model [40]. Later on, the use of polarized neutrons yielded a clear observation of the pinch points by isolating the "spin flip" cross section ([44] and Fig. 5), which entails most of magnetic modulations. In classical spin ice, flips of magnetic moments violating the ice rules can propagate along Dirac strings with low energy cost, leading to a separation of emergent magnetic charges akin to magnetic monopoles [45]. Such excitations are thermally activated and contribute to the diffuse scattering. Under magnetic field, the monopoles diffuse along the field and make random walk in the perpendicular plane, yielding specific features in the diffuse scattering, which were actually observed in $Dy_2Ti_2O_7$ [46].

From theory, starting from the classical spin ice and introducing transverse terms in the energy yields quantum spin ice behaviour, which allows tunnelling processes between spin configurations respecting the ice rules [47]. Accordingly, a unique quantum spin ice ground state with vanishing entropy at $T = 0$ could be built from a coherent superposition of large number of classical spin ice configurations. As a consequence of these quantum fluctuations, a new type of excitation has been predicted, quantum analogue of the monopoles, and associated with an emergent electromagnetic field. This "emergent photon" has not been observed up to now and constitutes a challenge of inelastic neutron scattering. Diffuse scattering experiments are also a crucial test for the quantum spin ice behaviour. The predicted diffuse scattering maps show the suppression of the pinch points by quantum fluctuations at

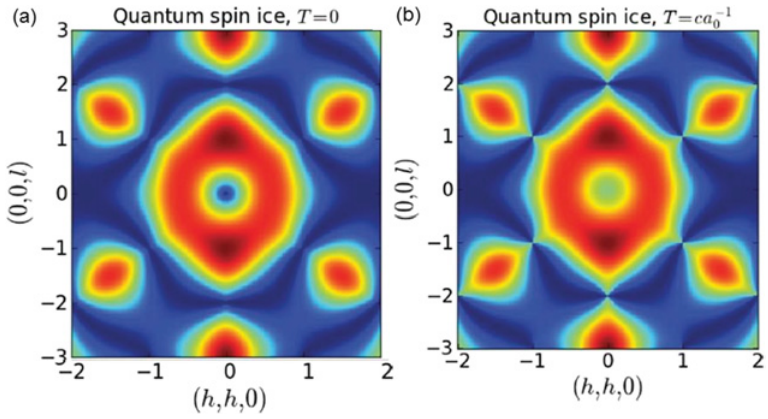

Figure 6. Predicted quantum spin ice behaviour as shown on diffuse scattering maps. a) at T = 0: the pinch points previously observed in classical spin ice are supressed by quantum fluctuations. In b) when increasing temperature, they are progressively restored by new excitations, called "emergent photons". From [47].

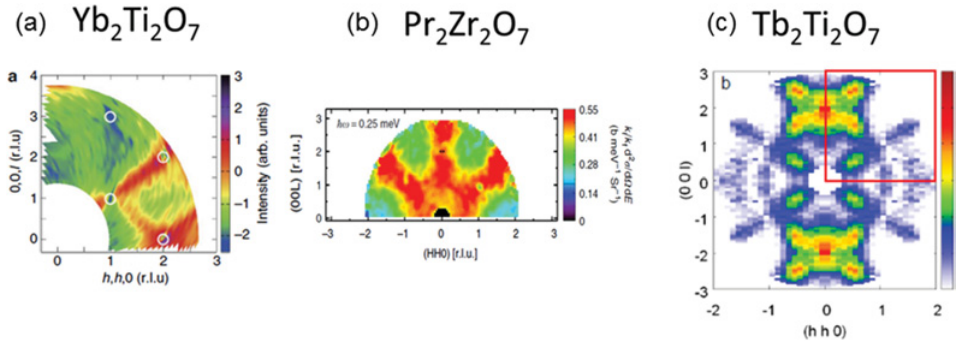

Figure 7. Single crystal neutron diffuse scattering maps in the (hh0, 00l) plane of the quantum spin ice candidates: a) $Yb_2Ti_2O_7$, from Ref. [48]; b) $Pr_2Zr_2O_7$, from Ref. [49]; c) $Tb_2Ti_2O_7$, from Ref. [50].

T = 0 and their progressive restoration with increasing temperature by the "emergent photons" (Fig. 6).

Experimentally, several routes towards quantum spin ice behaviours are possible, involving low magnetic moments, low energy crystal field levels, and/or quadrupolar interactions. Several pyrochlore materials such as $Yb_2Ti_2O_7$, $Tb_2Ti_2O_7$ and $Pr_2Zr_2O_7$ are presently considered as quantum spin ice candidates. None of them actually showed the behaviour predicted theoretically, but each of them offered an interesting and original variant to the classical spin ice behaviour, which can be seen on the diffuse maps at very low temperatures. In $Yb_2Ti_2O_7$, where Yb is a Kramers ion mapped to S=1/2, the polarized neutrons diffuse scattering maps show diffuse rods with features reminiscent of pinch points at <111> positions (Fig. 7a). This diffuse scattering becomes suppressed at $T_C = 0.2$ K when a first order transition settles in towards a ferromagnetic-like state, with low ordered magnetic moment and hysteretic features [48]. In $Pr_2Zr_2O_7$ where Pr is a non Kramers ion, similar broad features can be observed along the 111 directions, fully smearing the pinch points, and the modulations of the diffuse scattering occur in the inelastic channel, in a small energy range [49] (Fig. 7b).

$Tb_2Ti_2O_7$ spin liquid (Fig. 7c) offers the most complex and challenging alternative to classical spin ice behaviour. The diffuse scattering maps show well defined pinch points at the 111 positions, but with respect to $Ho_2Ti_2O_7$ and $Dy_2Ti_2O_7$ classical spin ices, the spectral weight is transferred out of the zone centre, and the intensity of the 200 diffuse peak explodes in a butterfly shape, with a dominant spectral weight on ½ ½ ½ and equivalent positions [50–52]. This antiferromagnetic version of the Coulomb phase suggests conservations rules holding over larger scales than a tetrahedron. Interestingly this disordered fluctuating ground state holds anisotropic excitations, which propagate perpendicular to the pinch points. Diffuse scattering combined with polarization and energy analysis of the transmitted neutron beam, yielded a clean determination of these exotic excitations, showing that their dispersion does not reflect that predicted for the emergent photon. The quantum spin ice state predicted by theoreticians therefore remains to be found.

6. Conclusion

This chapter summarizes some diffuse neutron scattering studies, focusing on local order in binary alloys and magnetic correlations in spin ices. These cases are only a few among the numerous fields of condensed matter physics which benefit from this approach. High luminosity spectrometers, polarization or energy analysis of the scattered neutrons, studies in extreme conditions of temperature, pressure, magnetic or electric field, should enable further studies in various domains, requiring sophisticated models and theories.

References

[1] J.M. Cowley, J. Appl. Phys. **21**, 24 (1950); B.E. Warren, X ray diffraction Courier Corp. (1969)
[2] B. Borie, C.J. Sparks, Acta Cryst. A **27**, 198 (1971)
[3] F. Frey, Mat. Sc. Engi. A. **294-296**, 178 (2000) QC; B. Toudic et al., Science **319**, 69 (2008)
[4] W. Marshall, S.W. Lovesey, Theory of thermal neutron scattering (Clarendon Press, 1971)
[5] S.M. Yusuf et al., Phys. Rev. B **82**, 094410 (2010)
[6] C. Ruegg et al., Phys. Rev. Lett. **93**, 037207 (2004)
[7] H. Yoshisawa et al., J. Phys. Soc. Jpn. Lett. SJ **57**, 3686 (1988)
[8] T. Fennell SFN **13**, 04001 (2014)
[9] `www.ill.eu/fr/instruments-support/instruments-groups/instruments/d7/description/`
[10] I.A. Blech, B.L. Averbach, Phys. Rev. B **137**, 1113 (1965); J. Davidowski et al., Neutron news **25**, 21 (2015)
[11] K.D. Rouse, M.J. Cooper Acta Cryst. A **26**, 682 (1970); A.W. Hewatt, Acta. Cryst. A **35**, 248 (1979)
[12] V.F. Sears, Neutron scattering lengths and cross sections tables, Neutron News **3**, 26 (1992)
[13] I. Mirebeau, M. Hennion, G. Parette Phys. Rev. Lett. **53**, 687 (1984); I. Mirebeau and G. Parette Phys. Rev. B **82**, 104203 (2010)
[14] M.E. Collins, Magnetic Critical Scattering; Oxford Series on Neutron Scattering in Condensed Matter
[15] E. Burkel et al., Z. Phys. B **35**, 227 (1979)
[16] S.E. Dutton et al., Phys. Rev. Lett. **108**, 187206 (2012)

[17] F. Bley, P. Cenedese, S. Lefebvre, AIP Conference Proceedings **89**, 276 (1982)
[18] E. Kentzinger et al., Phys. Rev. B **61**, 14975 (2000)
[19] V. Pierron-Bohnes et al., Phys. Rev. B **51**, 5760 (1995)
[20] T. Mehaddene et al., Eur. Phys. J. B **41**, 207 (2004)
[21] T. Priem et al., J. de Phys. **50**, 2217 (1989)
[22] R.A. Medina, J.W. Cable Phys. Rev. B **15**, 1539 (1977); H.R. Child and J.W. Cable Phys. Rev. B **13**, 227 (1976)
[23] J.E. Greedan et al., Phys. Rev. B **79**, 014427 (2009)
[24] A. Apetrei et al., Phys. Rev. Lett. **97**, 206401 (2006)
[25] I.V. Solovyev Phys. Rev. B **67**, 174406 (2003)
[26] J.E. Greedan et al., Phys. Rev. B **43**, 5682 (1991); J.N. Reimers Phys. Rev. B **46**, 193 (1992)
[27] FullProf, `http://www.ill.eu/sites/fullprof`
[28] P. Bordet SFN **9**, 139 (2008)
[29] B.A. Frandsen, X. Yang, S.J. Billinge, Acta Crystallogr. A **70**, 3 (2014)
[30] J.A.M. Paddison, A.L. Goodwin, Phys. Rev. Lett. **108**, 017204 (2012)
[31] R. Kikuchi, Phys. Rev. **81**, 988 (1951); J.M. Sanchez, V. Pierron-Bohnes and F. Mejia-Lira Phys. Rev. B **51**, 3429 (1995)
[32] S.T. Bramwell, M.J.P. Gingras Science **294**, 5546 (2001)
[33] M.J.P. Gingras, P.A. Mac Clarty, Rep. Prog. Phys. **77**, 056501 (2014)
[34] F. Ducastelle, F. Gautier, J. Phys. F **6**, 2039 (1976)
[35] M.Yu. Lavrentiev et al., Phys. Rev. B **75**, 014208 (2007)
[36] P. Erhart, A. Caro, M. Serrano de Caro, B. Sadigh, Phys. Rev. B **77**, 134206 (2008)
[37] P.C. Clapp, S.C. Moss, Phys. Rev. **171**, 754 (1968)
[38] M. Hennion, J. Phys. F **13**, 2351 (1983)
[39] A.V. Ruban, P.A. Korzhavyi, B. Johansson, Phys. Rev. B **77**, 094436 (2008)
[40] S. Bramwell et al., Phys. Rev. Lett. **87**, 047207 (2011)
[41] A.P. Ramirez et al., Nature (London) **399**, 333 (1999)
[42] R. Moessner, J.T. Chalker, Phys. Rev. B **58**, 12049 (1998)
[43] S.V. Isakov et al., Phys. Rev. Lett. **93**, 167204 (2004); C.L. Henley, Phys. Rev. B **71**, 014424 (2005)
[44] T. Fennell et al., Nat. Phys. 3, 566 (2007); Science **326** 415 (2009)
[45] C. Castelnovo, R. Moessner, S.L. Sondhi, Nature **451**, 42 (2008); I.A. Ryzhkin, M.A. Ryzhkin, JETP Lett. **93**, 384 (2011); C.L. Henley, Phys. Rev. B **71**, 014424 (2005)
[46] D.J.P. Morris et al., Science **326**, 411 (2009)
[47] O. Benton, O. Sikora, N. Shannon, Phys. Rev. B **86**, 075154 (2012)
[48] L.J. Chang et al., Nat. Comm. **3**, 992 (2012)
[49] K. Kimura et al., Nat. Comm. **4**, 1934 (2013)
[50] S. Petit et al., Phys. Rev. B **86**, 174403 (2012); S. Guitteny et al., Phys. Rev. Lett. **111**, 087201 (2013)
[51] T. Fennell et al., Phys. Rev. Lett. **109**, 017201 (2012)
[52] K. Fritsch et al., Phys. Rev. B **89**, 094410 (2013)